

## Vortex–lattice guided motion on isotropic and anisotropic artificial pinning landscapes

J.E. Villegas<sup>a,\*</sup>, E.M. González<sup>a</sup>, M.I. Montero<sup>b</sup>, Ivan K Schuller<sup>b</sup>, J.L. Vicent<sup>a</sup>

<sup>a</sup> *Departamento. Física de Materiales, Facultad de Ciencias Físicas, Universidad Complutense, 28040 Madrid, Spain*

<sup>b</sup> *Department of Physics, University of California-San Diego, La Jolla, California CA 92093-0319, USA*

### Abstract

Vortex–lattice dynamics has been studied in superconducting Nb thin films with periodic arrays of magnetic pinning centers. Magnetotransport measurements have been used to study vortex–lattice velocity as a function of the in-plane direction of the driving force. This has been done for samples with arrays of decreasing anisotropy, from rectangular arrays (two-fold symmetry) to square arrays (four-fold symmetry). Strongly guided vortex motion along privileged directions has been found in the former, but not in the latter. The results are discussed in terms of channeling effects.

© 2005 Elsevier Ltd. All rights reserved.

### 1. Introduction

Vortex–lattice dynamics on artificially induced pinning landscapes has attracted increasing interest during the last years. With the new nano-lithography techniques, it has become possible patterning superconducting thin films with ordered arrays of nano-objects (antidots, blind holes, magnetic, metallic or insulating dots, etc.) [1]. The characteristic lengths of these ordered arrays, such as the dots diameter or the lattice parameter of the arrays, are controllable within the submicrometric scale. This is the size of the relevant lengths governing the pinning of vortices, i.e. the coherence length  $\xi_S$  and the penetration length  $\lambda$ , what makes that these arrays of nano-dots create a very efficient pinning potential for the vortex–lattice. As a result, by patterning superconducting thin films with these artificial arrays, one may literally *design* the pinning potential landscape for the vortex–lattice.

There are a number of interesting phenomena arising in these nano-patterned superconductors, as for instance commensurability effects [2–6]. In these effects, the geometric matching between the vortex–lattice and the underlying periodic pinning potential strongly pins the vortex lattice, what yields enhanced critical currents [5] (or reduced dissipation [6]). Another interesting related issue has emerged recently: the possibility of reliably controlling the vortex–

lattice motion by using suitable pinning potential landscapes. For instance, it has been shown that asymmetric (*ratchet*) pinning potentials rectify vortex dynamics, in the sense that a net flow of the vortex–lattice arises when a not biased *ac* driving force is applied to it [7].

In this paper, we report on another kind of experiments, also related with the issue of controlled vortex motion. In particular, we report on guided vortex motion along privileged directions, which are defined by arrays of magnetic dots. We have previously reported [8] that, in Nb thin films with rectangular arrays of magnetic dots, guided vortex motion develops along directions far away from the direction of the applied driving force. In the present paper, we study this effect as a function of the anisotropy of the array of magnetic dots. Magnetotransport experiments have allowed us studying Vortex–lattice velocity as a function of the direction of the applied driving force (Lorentz force). We have performed these experiments for arrays with different decreasing anisotropy, from rectangular arrays (two-fold symmetry) to square arrays (four-fold symmetry), and also as a function of the applied magnetic field. We will show that guided vortex motion progressively smears out as the anisotropy of the array is reduced.

### 2. Experimental

Periodic arrays of magnetic (Ni) dots were fabricated using e-beam lithography techniques on Si (100), following the usual steps [1]. Ni thickness (dots height) is 40 nm and a superconducting Nb film 100 nm thick covers them. We have fabricated arrays with different symmetries: samples A and B

\* Corresponding author

E-mail address: [jeville@fis.ucm.es](mailto:jeville@fis.ucm.es) (J.E. Villegas).

have rectangular arrays (two-fold symmetry), with lattice parameters  $a \times b = 400 \times 500 \text{ nm}^2$  and  $a \times b = 400 \times 625 \text{ nm}^2$ , respectively [see Fig. 1(a)] whilst sample C has a square array (four-fold symmetry), with lattice parameters  $a \times b = 500 \times 500 \text{ nm}^2$  [see Fig. 1(b)]. Dots diameter is for all samples  $\phi = 200 \text{ nm}$ . Critical temperatures were  $T_c = 8.75 \text{ K}$  for sample A,  $T_c = 8.63 \text{ K}$  for sample B and  $T_c = 8.40 \text{ K}$  and for sample C.

Magnetotransport experiments (dc) were done in a liquid He cryostat provided with a superconducting magnet and a variable temperature insert that allows controlling temperature with stability of 1 mK. The magnetic field was applied perpendicular to the film plane and thus always perpendicular to the injected transport current. Samples were patterned with a cross-shaped measuring bridge by using optical lithography and ion-etching. This bridge allows injecting in the sample two crossing currents ( $J_x$  and  $J_y$ ), and also simultaneously measuring with two nanovoltmeters the voltage drops along two perpendicular directions  $V_x = V_3 - V_2$  and  $V_y = V_1 - V_2$  [see Fig. 1(c)]. With this arrangement, we can control the direction and intensity of the driving force (Lorentz force) on the vortex–lattice: taking into account  $\vec{F}_L = \vec{J} \times \vec{n} \phi_0$  (with  $\phi = 2.07 \times 10^{-15} \text{ Wb}$  and  $\vec{n}$  a unitary vector parallel to the applied magnetic field), each one of the orthogonal injected currents yield the components  $F_x = J_y \phi_0$  and  $F_y = J_x \phi_0$ . Therefore, the resulting magnitude of the driving force is  $F_L = \sqrt{F_x^2 + F_y^2}$  and its direction  $\theta = \arctan(F_x/F_y) = \arctan(J_y/J_x)$ . Using the expression for the electric field  $\vec{E} = \vec{B} \times \vec{v}$ , where  $\vec{B}$  is the applied magnetic field and  $\vec{v}$  the vortex–lattice velocity, we calculate the vortex–lattice velocity components  $v_j = V_j/(dB)$  from the measured voltage drops  $V_i$  (with  $d$  the distance between contacts). Thus we obtain the magnitude  $v = \sqrt{v_x^2 + v_y^2}$  and direction  $\alpha = \arctan(v_x/v_y)$  of the vortex–lattice velocity. A sketch with definition of angles and directions with respect to the lattice vectors of the array of dots is depicted in Fig. 1(d).

### 3. Results and discussion

The vortex–lattice velocity as a function of the applied magnetic field, but at constant temperature and constant magnitude of the driving force  $F_L$ , is shown in Figs. 2–4 for samples A, B and C, respectively. There are two panels in each one of those figures. In panel (a), the direction  $\alpha$  of the vortex–lattice velocity is shown, and in (b) its magnitude  $v$ , for several different directions  $\theta$  of the driving force.

The dc magnetoresistance in the mixed state of samples with periodic arrays of pinning centers exhibits well-known commensurability phenomena [6]. For given applied magnetic fields, geometrical matching between the vortex–lattice and the periodic pinning potential develops. At these matching fields, the interaction between the vortex–lattice and the array of magnetic dots is enhanced, i.e. the pinning force is optimized. Because of this the Vortex–lattice moves slower, yielding reduced dissipation.

Samples with two-fold symmetry A and B show two different regimes [see Fig. 2 (b) and Fig. 3(b)] concerning the matching fields. In the low-field regime, minima appear when magnetic field yields an integer number of vortices per unit cell; for sample B it is  $\Delta H_{\text{low}} = 104 \text{ Oe}$  ( $\Delta H = \phi_0/ab = 103 \text{ Oe}$ ), while it is  $\Delta H_{\text{low}} = 84 \text{ Oe}$  ( $\Delta H_{\text{low}} = \phi_0/ab = 82.9 \text{ Oe}$ ) for sample A. In the high-field regime, the minima corresponds to matching between the vortex–lattice parameter and the rectangular array short side  $a$ , showing up  $\Delta H_{\text{high}} = 122 \text{ Oe}$  for sample B and  $\Delta H_{\text{high}} = 130 \text{ Oe}$  for sample A (in quite good agreement with  $\Delta H_{\text{high}} = \phi_0/a^2 = 129 \text{ Oe}$ ). The transition between those two different regimes has been explained in terms of the reconfiguration in the vortex lattice from rectangular to square geometry [9]. Additionally, fractional matching effects [10] are present for sample B [see Fig. 3 (b)], for which swallow but clear minima appear at fields  $0.5\Delta H_{\text{low}} = 52 \text{ Oe}$  and  $1.5\Delta H_{\text{low}} = 156 \text{ Oe}$ . Matching fields do

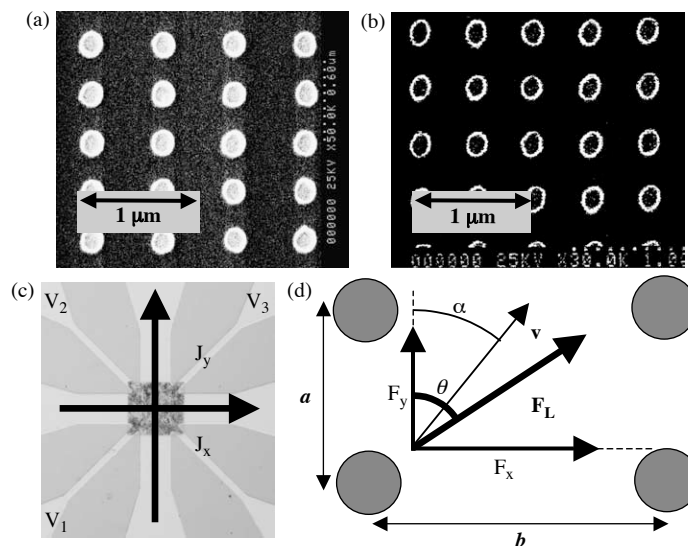


Fig. 1. (a), (b) SEM images of the arrays of samples A and C, respectively. (c) Micrograph of the measuring bridge. The area where currents cross is  $40 \times 40 \mu\text{m}^2$ , and the one containing arrays is  $90 \times 90 \mu\text{m}^2$  (darker region). (d) Sketch with notation and definition of angles and directions.

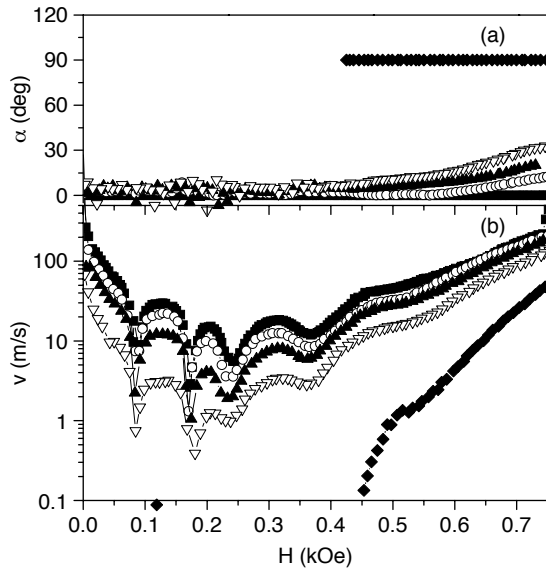


Fig. 2. Vortex–lattice velocity  $v$  and direction of motion  $\alpha$  for sample A ( $a \times b = 400 \times 625 \text{ nm}^2$ ) as a function of the applied magnetic field, at  $T = 0.98T_c$ , and applied driving force  $F_L = 5.17 \times 10^{-7} \text{ Nm}^{-1}$ , for different  $\theta = 0^\circ$  (black squares),  $30^\circ$  (hollow circles),  $45^\circ$  (black triangles),  $60^\circ$  (hollow triangles) and  $90^\circ$  (black diamonds).

not depend on the direction  $\theta$  of the driving force. However, the magnitude  $v$  of the vortex–lattice velocity strongly depends on  $\theta$ . For both samples A and B, at low applied magnetic fields, the vortex–lattice velocity is reduced more than one order-of-magnitude when the driving force is rotated from  $\theta = 0^\circ$  to  $\theta = 60^\circ$  [See Figs. 2(b) and 3(b)]. For  $\theta = 90^\circ$ , at low applied magnetic fields, the vortex–lattice velocity falls below measurable values at this magnitude  $F_L$  of the driving force. Moreover, as can be seen in Fig. 2(a) and Fig. 3(a), the

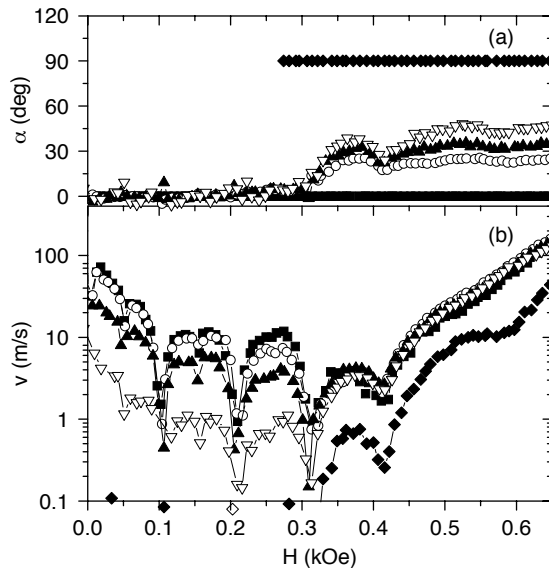


Fig. 3. Vortex–lattice velocity  $v$  and direction of motion  $\alpha$  for sample B ( $a \times b = 400 \times 500 \text{ nm}^2$ ) as a function of the applied magnetic field, at  $T = 0.99T_c$ , and applied driving force  $F_L = 2.58 \times 10^{-7} \text{ Nm}^{-1}$ , for different  $\theta = 0^\circ$  (black squares),  $30^\circ$  (hollow circles),  $45^\circ$  (black triangles),  $60^\circ$  (hollow triangles) and  $90^\circ$  (black diamonds).

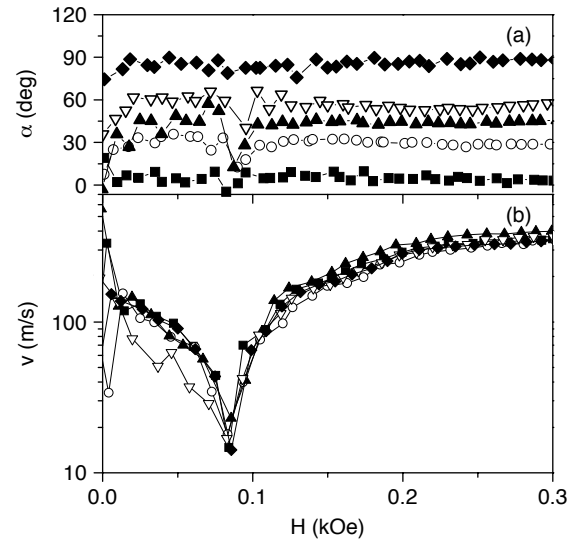


Fig. 4. Vortex–lattice velocity  $v$  and direction of motion  $\alpha$  for sample C ( $a \times b = 500 \times 500 \text{ nm}^2$ ) as a function of the applied magnetic field, at  $T = 0.995T_c$ , and applied driving force  $F_L = 2.58 \times 10^{-7} \text{ Nm}^{-1}$ , for different  $\theta = 0^\circ$  (black squares),  $30^\circ$  (hollow circles),  $45^\circ$  (black triangles),  $60^\circ$  (hollow triangles) and  $90^\circ$  (black diamonds).

direction of motion of the vortex–lattice  $\alpha$  is not parallel to the driving force  $\theta$ . In the low field regime,  $\alpha$  is locked in at  $\alpha = 0$  for all  $\theta$  i.e. vortex lattice moves guided along the short lattice-vector of the  $a$  of the rectangular array, even though the driving force is applied far away from it [8]. Easy-flow paths (channels) guiding the vortex–lattice lie along the direction whose inter-dots distance is smaller. The physical origin of these channels is the overlap of the pinning potential wells existing around each one of the magnetic dots in the array. The smaller is the inter-dots distance, the wider is the overlap, what yields the channels along the direction of the shortest lattice vector of the rectangular array [11]. The strongly guided vortex motion progressively smears out as magnetic field is increased. For sample A (the more anisotropic,  $a \times b = 400 \times 625 \text{ nm}^2$ ), Vortex–lattice velocity starts to rotate towards the direction of the driving force  $\alpha \rightarrow \theta$  above the fourth matching field ( $H \sim 0.4$  kOe), being  $\alpha$  progressively closer to  $\theta$  as magnetic field is increased. For sample B ( $a \times b = 400 \times 500 \text{ nm}^2$ ) the vortex–lattice motion is no longer locked in along channels above the third matching field ( $H \sim 0.3$  kOe). The fact that guided vortex motion is smeared out as applied magnetic field increases is expected. As  $H$  gets higher, vortices get closer, and vortex–vortex interactions become stronger, progressively washing out effects coming from the pinning potential.

For sample C (four-fold symmetry), local minima in the vortex–lattice velocity occurs when the applied magnetic field yields an integer number of vortices per unit cell of the array. Accordingly, minima are observed with period  $\Delta H = 80$  Oe [see Fig. 4(b)], in good agreement with the expected value  $\Delta H = \phi_0/ab = 82.8$  Oe (with  $a = b = 500$  nm). As can be seen the  $v(H)$  curves are similar for all the directions  $\theta$  of the driving force. Matching fields are independent on the direction  $\theta$  of the driving force. Also the magnitude of the vortex–lattice velocity

$v$  is similar for all angles  $\theta$ . In [Fig. 4(a)], the direction  $\alpha$  of the vortex–lattice velocity is shown as a function of the applied magnetic field. For this four-fold symmetry array, the vortex–lattice velocity is always essentially parallel to the direction of the driving force,  $\alpha \approx \theta$ , at all applied magnetic fields. That is, there is not guided vortex motion on the square array of magnetic dots. This is at variance to what was expected from theoretical simulations [12], and to the results reported from experiments on Pb thin films with square arrays of holes [13]. In these works, it was found that guided vortex motion develops along the main symmetry axes of the square array. The fact that this is not observed in our sample might be explained by assuming that the square array of magnetic dots produces identical easy-flow channels along two perpendicular directions, those of the lattice vectors  $a$  of the array. This is indeed expected from our results for the rectangular arrays. The existence of channels along two perpendicular directions would allow the vortex–lattice following the direction of the driving force, by conveniently switching in a zigzag motion from channels along one direction to channels along the other. Further experiments are required to clarify this scenario.

#### 4. Conclusions

We have studied vortex–lattice dynamics as a function of the direction of the driving force on pinning potential landscapes created by arrays on magnetic dots with different symmetries. In samples with rectangular arrays (two-fold symmetry), vortex dynamics is highly anisotropic, showing up strongly guided vortex motion along the short lattice-vector of the array. This effect is slowly smeared out as the applied magnetic field is increased. Samples with square arrays (four-fold symmetry), on the contrary, show up isotropic vortex

dynamics, in which the motion of the vortex–lattice essentially follows the direction of the driving force.

#### Acknowledgements

We want to thank Spanish MAT2002 - 04543, MAT2002-12385E, R. Areces Foundation, US NSF. One of us EMG wants to thank Spanish Ministerio de Educación y Ciencia for a Ramon y Cajal contract.

#### References

- [1] J.I. Martín, J. Nogués, K. Liu, J.L. Vicent, I.K. Schuller, *J. Magn. Magn. Mater.* 256 (2002) 449.
- [2] O. Daldini, P. Martinoli, J.L. Olsen, G. Berner, *Phys. Rev. Lett.* 32 (1974) 218.
- [3] A. Pruyboom, P.H. Kes, E. van der Drift, S. Radelaar, *Phys. Rev. Lett.* 60 (1988) 1430.
- [4] Y. Otani, B. Pannetier, J.P. Nozières, D. Givord, *J. Magn. Magn. Mater.* 126 (1993) 622.
- [5] M. Baert, V. Metlushko, R. Jonckheere, V.V. Moshchalkov, Y. Bruynseraede, *Phys. Rev. Lett.* 74 (1995) 3269.
- [6] J.I. Martín, M. Vélez, J. Nogués, Ivan K. Schuller, *Phys. Rev. Lett.* 78 (1997) 1929.
- [7] J.E. Villegas, S. Savel'ev, F. Nori, E.M. González, J.V. Anguita, R. García, J.L. Vicent, *Science* 302 (2003) 1188.
- [8] J.E. Villegas, E.M. González, M.I. Montero, I.K. Schuller, J.L. Vicent, *Phys. Rev. B* 68 (2003) 224504.
- [9] J.I. Martín, M. Vélez, A. Hoffmann, I.K. Schuller, J.L. Vicent, *Phys. Rev. Lett.* 83 (1999) 1022.
- [10] O.M. Stoll, M.I. Montero, J. Guimpel, J.J. Åkerman, I.K. Schuller, *Phys. Rev. B* 65 (2002) 104518.
- [11] M. Velez, D. Jaque, J.I. Martín, M.I. Montero, I.K. Schuller, J.L. Vicent, *Phys. Rev. B* 65 (2002) 104511.
- [12] C.C. de Souza Silva, G. Carniero, *Phys. Rev. B* 66 (2002) 054514.
- [13] A.V. Silhanek, L. Van Look, S. Raedts, R. Jonckheere, V.V. Moshchalkov, *Phys. Rev. B* 68 (2003) 214504.